DOE/NV/10412-10

RESERVOIR ENGINEERING STUDIES OF THE GLADYS McCALL GEOPRESSURED-GEOTHERMAL RESOURCE

THE UNIVERSITY OF TEXAS AT AUSTIN

CENTER FOR PETROLEUM AND GEOSYSTEMS ENGINEERING
CPGE

DISCLAIMER

Center for Petroleum and Geosystems Engineering

RESERVOIR ENGINEERING STUDIES OF THE GLADYS McCALL GEOPRESSURED-GEOTHERMAL RESOURCE

Final Report

by Chen-Min Lea, Kunsang Lee, and Mark A. Miller

Prepared for the U. S. Department of Energy
Advanced Technologies Division
under Cooperative Agreement No.DE-FC07-85NV10412

Department of Petroleum Engineering
The University of Texas at Austin
Austin, TX 78712

Report No. 93-6
September 1993

TABLE OF CONTENTS

LIST OF TABLES

LIST OF FIGURES

ABSTRACT

Transient pressure analysis techniques have been used to evaluate the performance of the Gladys McCall geopressured-geothermal reservoir. A fault-controlled aquifer influx model has also been developed to account for pressure support observed during both reservoir depletion and recovery phases.

The Gladys McCall No. 1 well was drilled and completed in the lower Miocene geopressured sandstones under the U.S. Department of Energy geopressured-geothermal research program. The well was shut in October 1987 after producing over 27 MMstb of brine and 676 MMscf gas since October 1983. Eight pressure transient tests were conducted in the well. Analysis of transient pressure data provided a quantitative evaluation of reservoir characteristics, including: a) formation transmissibility and skin, b) the size and possible shape of the main producing reservoir, and c) characteristics of the pressure support mechanism.

The pressure behavior of 1983 Reservoir Limits Test (RLT) suggested that the Gladys McCall reservoir might have a long narrow shape with the well located off-center. An elongated numerical model developed accordingly was able to reproduce the pressure characteristics shown in the test. During both the reservoir production and shut-in periods, pressure buildup tests indicated some degree of external pressure support. Aquifer recharging was believed to be the main source. Based on reservoir material-balance calculations, an aquifer influx model was derived from a conceptual model of water leakage through a partially sealing fault into the reservoir under steady-state conditions. Moreover, a match of the pressure history required that the conductivity of the fault be a function of the pressure difference between the supporting aquifer and the reservoir.

INTRODUCTION

The existence of subsurface regions having abnormally high formation pressures in many areas around the world has been known for a long time. These geopressured-geothermal aquifers are presumed to contain a large resource of natural gas in solution with the native brine. As part of its program to define the magnitude and recoverability of the geopressured/geothermal energy resource, the U.S. Department of Energy (DOE)

has drilled and tested 4 wells in Tertiary deposits of the northern Gulf of Mexico basin along the Texas and Louisiana coastal region (Wallace, 1982).

Our research has been directed to the Gladys McCall No. 1 well which lies at the western edge of the Rockefeller Wildlife Refuge about 55 miles southeast of Lake Charles in Cameron Parish, Louisiana. The geology of the Gladys McCall prospect was reviewed in detail by John (1988). The stratigraphic section seen in the borehole consists of an interbedded sequence of relatively thick sandstones and thin shales. There are approximately 1,100 ft of net sand in the target Miocene sand in the 14,412 ft to 15,860 ft interval penetrated. Sand Zone No. 8, from 15,158 ft to 15,490 ft with a gross section of 332 ft, was perforated and tested.

Production began on October 7, 1983, and the well produced over 27 MMstb of brine and 676 MMscf gas without any significant pressure decline. Although production from Gladys McCall No. 1 included numerous rate changes, the production history may be divided into two major phases. Except for relatively short time intervals, the bottomhole pressure generally decreased to April 21, 1987 (depletion phase). During this period, the average flow rate (q_p) was 19,600 stb/day. Starting on April 21, 1987, the flow rate of the well was lowered to 9,800 stb/day until the initiation of a multi-rate drawdown test on October 24, 1987. The well was shut in on October 29, 1987 in order to monitor the pressure recovery. The pressure increased during the 191 day period of reduced flow rate, and continued to increase following shut-in (recovery phase). On October 10, 1991, the well was reopened to conduct an additional short-term drawdown test.

This report contains three studies. First is an evaluation of existing correlations to predict brine properties as functions of temperature and pressure. Second is an analysis of pressure transient data from the eight tests to evaluate the size and shape of the reservoir, along with transmissivity (kh), permeability (k), skin factor (S), and average reservoir pressure (p_r). The third studt was an evaluation of the reservoir drive mechanism using long-term pressure data. Earlier studies (Riney, 1988 and 1990) believed that cross-flow from an overlying sand was the predominant drive mechanism. We found the pressure support to be acting like a steady-state aquifer influx, however, insufficient data were available to determine its spatial location. The amount of water influx across some exterior reservoir boundary was estimated using reservoir pressure

data obtained from the buildup tests. Results of the analyses furnished a quantitative evaluation of the reservoir and a better understanding of the reservoir energy drive mechanism.

RESERVOIR FLUID PROPERTIES

Values of reservoir brine properties are often needed when laboratory PVT data are not available. Accurate knowledge of the physical properties of water is important for predicting behavior of geopressured-geothermal reservoirs. This study involves an evaluation of literature information on physical properties of brine and comparison of the correlation results with experimental values.

When making reservoir calculations, the physical properties most frequently needed are viscosity (μ_w), density (ρ_w), compressibility (C_w), and formation volume factor (B_w). Weatherly Laboratories, Inc. of Lafayette, Louisiana reported properties of Gladys McCall fluid samples recombined to approximate reservoir conditions. The bubble point pressure (p_b) was determined to be 9,200 psia with a dry gas-water ratio of 31.6 scf/stb. The average total gas production from the test well is about 30.15 scf/stb. The reservoir fluid viscosity and compressibility were measured to be 0.31 cp and 2.76×10^{-6} psi^{-1}, respectively, at initial reservoir conditions (12,784 psia and 289.2 °F at 12,100 ft). Average salinity of the brine is 97,800 mg/liter.

Reservoir brine properties were predicted with available correlations as function of temperature, pressure, and salinity. Despite the fact that natural gas is soluble in brines, little useful data have been published regarding the effect of dissolved gas on brine properties. Since reservoir water contains dissolved salts, the effect of salt concentration must be included. Reservoir waters generally contain, in addition to sodium chloride ($NaCl$), various other salts such as potassium chloride (KCl), sodium carbonate (Na_2CO_3), calcium chloride ($CaCl_2$), magnesium chloride ($MgCl_2$), and calcium sulfate ($CaSO_4$). The other salts, however, are present in small enough concentration that they can often be treated as sodium chloride equivalents. This was the approach used here. The mass fraction composition employed to represent the Gladys McCall brine is as follows (Riney, 1990):

H_2O: 0.904179 CH_4: 0.003481 $NaCl$: 0.092340

To calculate the compressibility, we used Osif's (1984) and Meehan's (1980) correlations (Fig. 1). The results of the two calculations are almost identical and slightly lower than the experimental value. Formation volume factor was estimated with McCain's (1990), Numbere's (1977), Horne's (1990), and Kutasov's (1991) correlations (Fig. 2). Estimated values show small deviation from laboratory data. Calculated values of methane solubility in hot brines are a little lower than the experimental values (Fig. 3). The viscosity correlations show relatively large differences (Fig. 4). It is unknown why such large differences exist. This needs to be investigated further. Meehan's correlation matches the laboratory data best.

As shown in Figs. 1 to 4, the results of the various correlations compare fairly well with results of actual reservoir fluid analysis reported by Weatherly Laboratory, Inc. Generally differences are less than 10%.

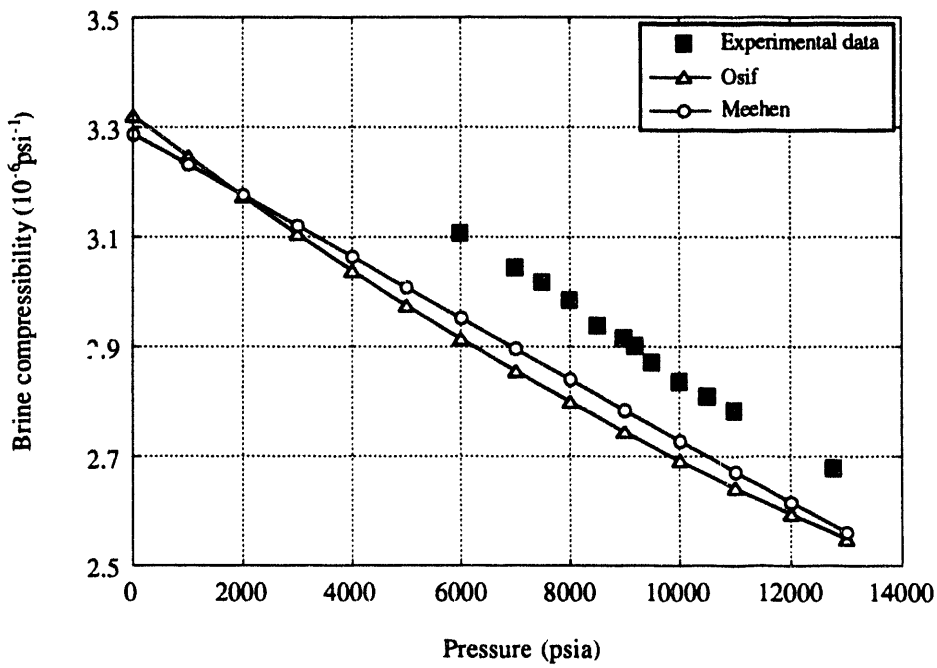

Fig. 1: Brine compressibility vs. pressure for Gladys McCall brine at 289.2°F.

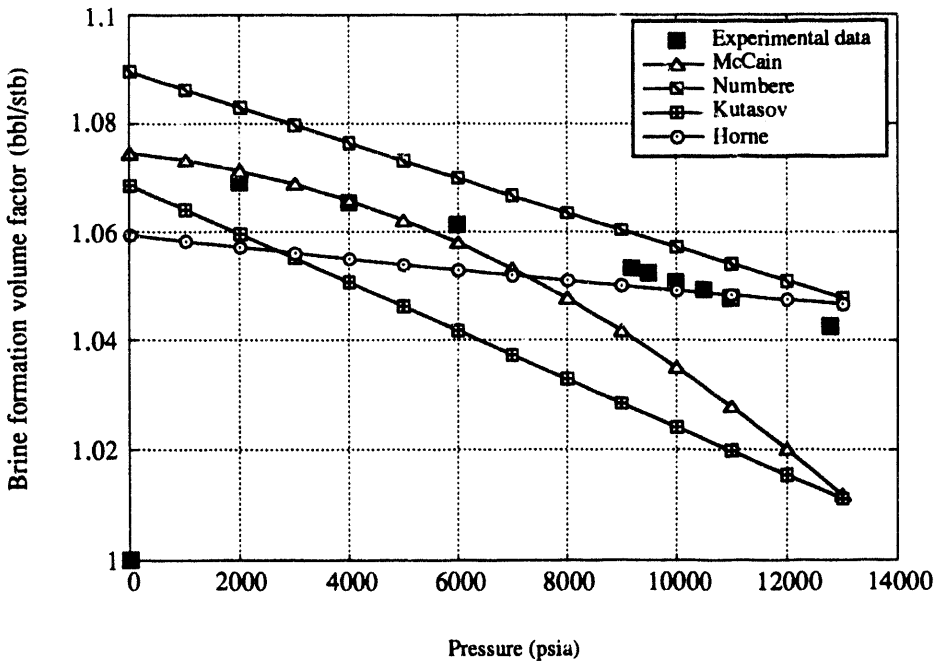

Fig. 2: Brine formation volume factor vs. pressure for Gladys McCall brine at 289.2°F.

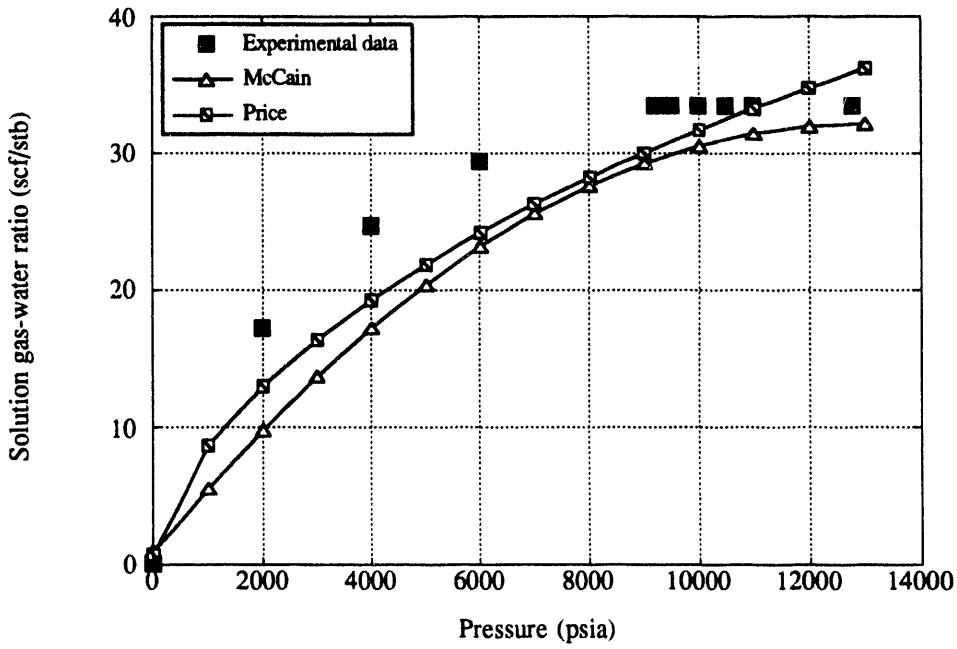

Fig. 3: Saturated solution gas-water ratio vs. pressure for Gladys McCall brine at 289.2°F.

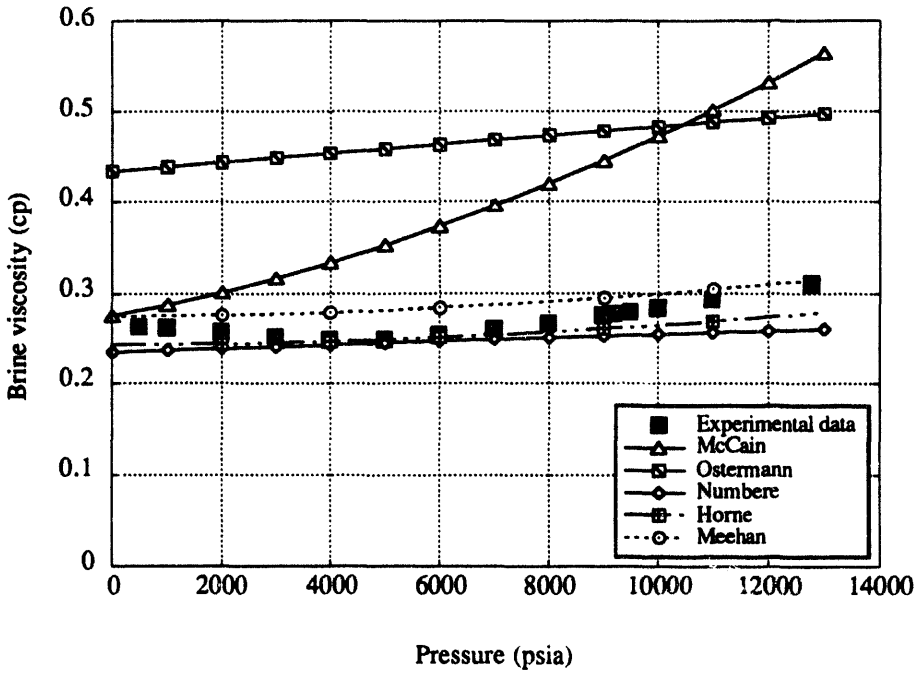

Fig. 4: Brine viscosity vs. pressure for Gladys McCall brine at 289.2°F.

TRANSIENT PRESSURE ANALYSIS

Eight pressure drawdown and buildup tests were conducted in the Gladys McCall No.1 well from October 1983 to October 1991. Subsurface pressure responses of all tests were reanalyzed to get as much reservoir data as possible. Analysis of the data furnished a preliminary reservoir description such as the formation parameters, pore volume and shape of the reservoir, and average reservoir pressure.

Bottomhole pressure transient measurements consist of a Reservoir Limits Test (drawdown and buildup, October 1983), 79-hour buildup (April 1985), 92-hour buildup (January 1986), Long-Term Test (drawdown and buildup, October 1987), and '91 Test (drawdown and buildup, October 1991). The flow stream, at bottomhole conditions, contained no free gas because wellbore pressure was always higher than the bubble point pressure. It is, therefore, felt that single phase analysis methods should be adequate to analyze the pressure transient data.

Transient Pressure Analysis

The important formation and fluid properties employed in the transient pressure test calculations are:

Reservoir thickness (h) = 332 ft

Average porosity (ϕ) = 0.16

Total system compressibility (C_t) = 6.27×10^{-6} psi^{-1}

Water viscosity (μ_w) = 0.31 cp

Water formation volume factor (B_w) = 0.984 bbl/stb

Wellbore radius (r_w) = 0.2917 ft

At early times of a well test, pressure responds as if the well is flowing in an infinitely large reservoir. Formation transmissivity, kh, is usually analyzed from this radial-flow period by measuring the slope, m, of a semi-log drawdown plot (p_{wf} vs. $log\ t_p$) or Horner buildup plot (p_{ws} vs. $log\ (t_p+\Delta t)/\Delta t$) (Earlougher, 1977). Later in the test, when part or all of the reservoir boundaries are felt at the well, other reservoir flow regimes may be encountered, such as linear flow, pseudosteady-state flow, and flow with aquifer influx support. Appropriate reservoir models are then selected to evaluate the reservoir parameters (size, shape, well distance to sealing fault, etc.) that bring about the observed flow characteristics. This will be discussed in subsequent sections.

For better diagnosing the pressure transient data, pressure derivative plots are now widely used. These plots highlight and emphasize the dominant flow regimes in a transient test (Bouret Ital., 1985; Ehlig-Economides, 1988). The pressure derivative interpretation is based on the analysis of the pressure changes with respect to time. Each reservoir flow regime has its own distinguishable derivative pattern. For example, a semilog plot of the Reservoir Limits Drawdown wellbore pressure vs. time yields a straight line from 0.2 hr to 0.7 hr, shown in Fig. 5, indicating early radial flow. The occurrence and duration of this infinite acting period can be easily confirmed from the first horizontal portion of the pressure derivative log-log plot, as illustrated in Fig. 6. Figure 6 also indicates the possible existence of a second infinite acting period and clear

influence of outer boundary effects. Detailed analysis of the Reservoir Limits Tests using combined information of pressure and pressure derivative responses will be presented in the numerical model simulation section. The pressure derivative formula used in this study is given in Horne (1990).

Results of all bottomhole pressure transient measurements and evaluations for the Gladys McCall reservoir are summarized in Table 1. All pressure transient (buildup) tests subsequent to the Reservoir Limits Test show a reduction of transmissivity values. An earlier study (Riney, 1990) assumed that this reduction in transmissivities was attributed to partial plugging of Sand Zone No. 8 in conjunction with a shale stringer identified from well logs at a depth of 15,365 to 15,369 ft. This has not been verified. Another common feature among the buildup tests is that their pressure derivative plots, as illustrated in Appendix A, show characteristics of an apparent increasing kh (dip in derivative curves) during the infinite acting period. This behavior could indicate one of the following: 1. Wellbore is partially damaged with damage extending some depth into the formation 2. Reservoir is composed of commingled layers with contrast layer permeabilities 3. Reservoir anisotropy 4. Pressure support from nearby partially leaking fault system. We tried a few numerical models simulating some of above situations and achieved some matched results. However, because of insufficient hard data it would not be useful to obtain an exact match with only speculative causes. Appendix A illustrates some of the results.

The skin factor (S) was computed from the pressure drawdown and buildup equations as documented by Earlougher (1977). Skin factors ranged from 2.2 to 6.8. Abrupt increases in skin factor are believed to be associated with injection of a scale inhibitor pill. The high values of skin factor have also been attributed to precipitates forming in the formation pores (Riney, 1990). Flow of brine through the formation has apparently flushed out the precipitates in the pores thereby decreasing skin values.

The Reservoir Limits Drawdown Test was analyzed to determine the reservoir volume communicating with the well. Pressure during pseudosteady-state flow declines linearly by (Earlougher, 1977):

$$p_{wf} = -m^*t + p_{int} \qquad (1)$$

where

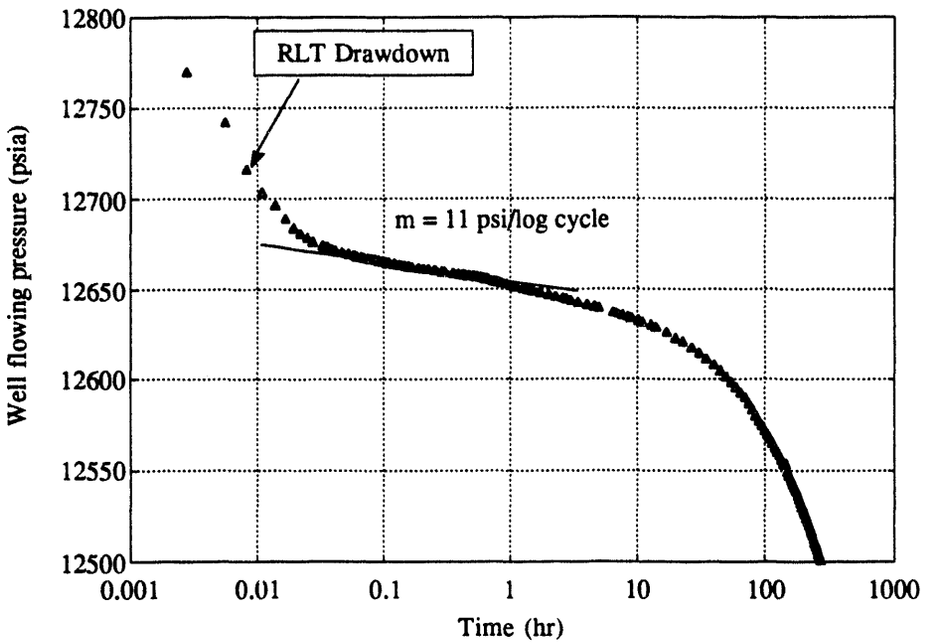

Fig. 5: 1983 Reservoir Limits Test drawdown wellbore pressure vs. flowing time.

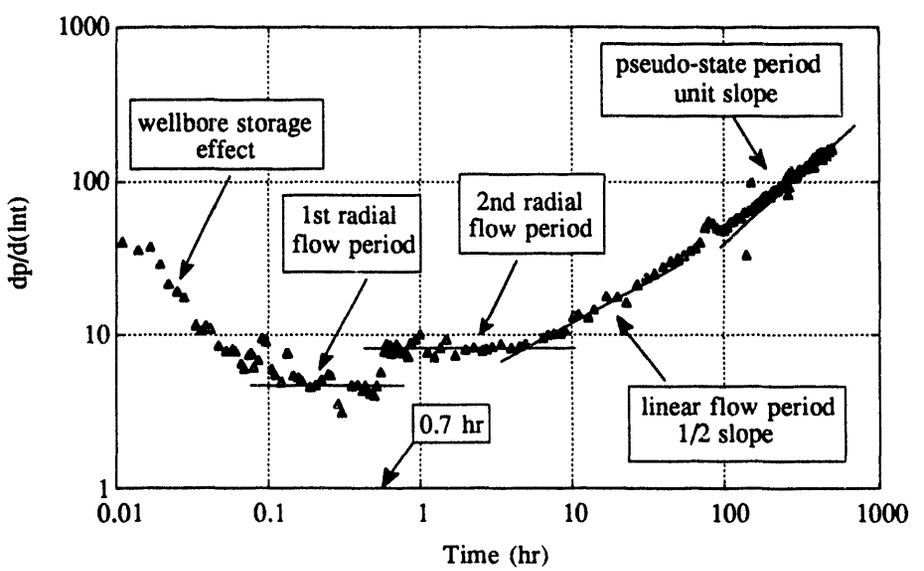

Fig. 6: 1983 Reservoir Limits Test drawdown pressure derivative plot.

Table 1: Summary of results of bottomhole pressure transient measurements for Gladys McCall Well No.1.

Permeability (k)

	Reservoir Limits Test (RLT)		79-Hour	92-Hour	Long-Term Test		'91 Test	
	Draw-down	Buildup	Buildup	Buildup	Draw-down	Buildup	Draw-down	Buildup
Date	Oct 07 '83	Oct 28 '83	Apr 09 '85	Jan 23 '86	Oct 25 '87	Oct 29 '87	Oct 10 '91	Oct 14 '91
Test Days (day)	0	21	550	839	1,479	1,483	2,924	2,928
Q (10^3 sep bbls)	0	298	7,788	13,951	27,131	27,182	27,182	27,206
$[p_{wf}]_{0\ hr}$ (psia)	12,784	12,418	10,855	10,267	10,068	10,074	12,096	11,981
q_P(stb/day)	14,162	14,162	15,438	10,470	5,100	9,950	5,975	5,975
m (psi/cycle)	-11	-15.5	-29.5	-19		-15	-9.25	-9.5
kh (md-ft)	43,901	45,318	25,957	27,332		32,901	31,908	31,196
k (md) (h=332 ft)	201.2	136.5	78.2	82.3		99.1	96.1	94.0
k (md) (h=207 ft)			125.4	132.0		158.9	154.1	150.7

Skin Factor (S)

	Reservoir Limits Test		79-Hour	92-Hour	Long-Term Test		'91 Test	
	Draw-down	Buildup	Buildup	Buildup	Draw-down	Buildup	Draw-down	Buildup
p_{1hr}	12,655	12,557	11,213	10,463	—	10,229	12,017	12,059
S (h=332 ft)	2.194	2.846	6.766	4.665	—	4.592	2.544	2.175
S(h=207 ft)			6.530	4.429	—	4.356	2.308	1.939

$$m^* = \frac{0.234\, q_w B_w}{\phi C_t h A} \tag{2}$$

and the pressure at intercept (time =0 hr), *Pint* is:

$$p_{int} = p_i - \frac{70.6\, q_w B_w \mu_w}{kh}\left[ln\left(\frac{A}{r_w^2}\right) + ln\left(\frac{2.2458}{C_A}\right) + 2s \right] \tag{3}$$

The slope can be used to estimate the connected reservoir drainage volume (V_p).

$$V_p = \phi h A = \frac{0.234\, q_w B_w}{C_t m^*} \tag{4}$$

The pseudosteady-state period and time at the beginning of pseudosteady-state flow (t_{pss}) were determined by using both Cartesian and derivative plots. A closed outer boundary shows a steeply-rising straight line of unit slope on derivative plot (Fig. 6). From Fig. 7, a Cartesian plot of wellbore flowing pressure, pseudosteady-state flow begins at around 300 hrs. The rate of change in p_{wf} with time (dp_{wf}/dt) is 0.3471 psi/hr, and the pressure at intercept (p_{int}) is 12,592 psi. From the above relationships, the estimated pore volume of reservoir is about 2.70×10^8 bbls. Riney's (1990) reservoir simulation model had a volume of 2.45×10^9 bbls below an overlying sand, which includes the surrounding aquifer as part of the reservoir. We treat the pressure-supporting aquifer as a separate system.

The results of the Reservoir Limit Test were also used to estimate the drainage shape for the well. The system shape factor (C_A) can be estimated from (Earlougher, 1977):

$$C_A = 5.456\left(\frac{m}{\pi}\right)\exp\left[\frac{2.303\,(p_{1hr} - p_{int})}{m}\right] \tag{5}$$

and

$$(t_{DA})_{pss} = 0.1833\left(\frac{m^*}{m}\right) t_{pss} \tag{6}$$

where

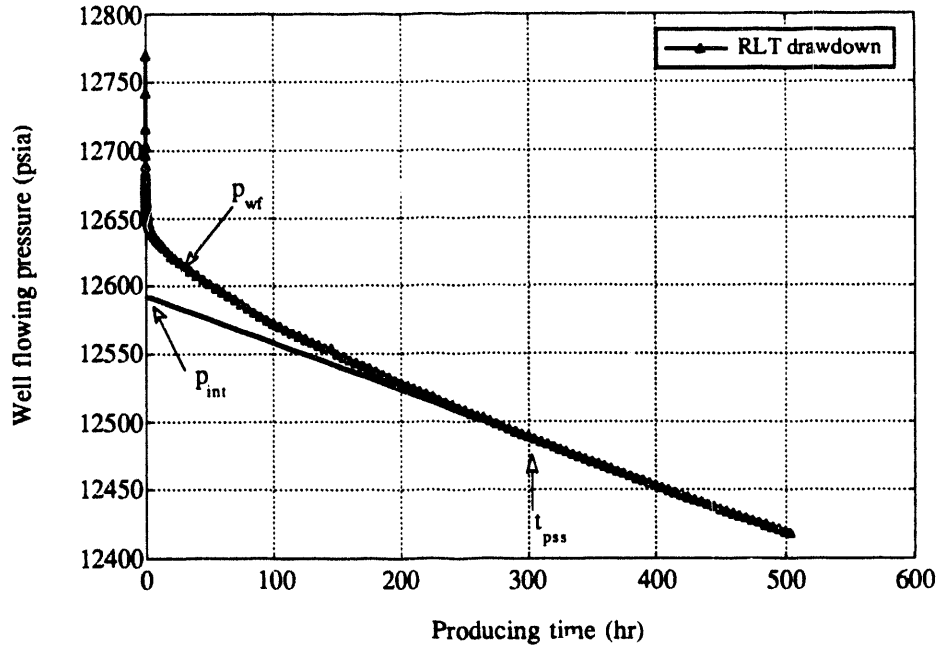

Fig. 7: Cartesian plot of Reservoir Limits drawdown test.

m = slope of linear portion of semilog plot (psi/cycle)

m^* = slope of straight line on a linear plot of p_{wf} vs. t (psi/hr)

$$(t_{DA})_{pss} = \frac{0.0002637\, kt_{pss}}{\phi \mu_w C_t A} \tag{7}$$

= dimensionless time at the beginning of pseudosteady-state flow

Using plots of the drawdown test (Figs. 6 and 7) and the above equations, we estimated $C_A = 6.0\text{x}10^{-2}$ and $(t_{DA})_{pss} = 1.19$. Also pressure data were compared with type curves of single-well rectangular systems presented by Earlougher and Ramey (1973). The closest shape found was 4:1 rectangular drainage area with well located near one corner. From these analyses, it can be postulated that the reservoir has a long and narrow shape, probably with the well significantly off-center.

For all of the buildup tests, the flow period was sufficiently long to reach pseudosteady-state conditions. Therefore, average reservoir pressure (p_r) was calculated

by using the Matthews, Brons, and Hazebroek (MBH) technique (Dake, 1978):

$$p_{D(MBH)} = 0.01416 \frac{kh}{q_n \mu_w B_w} (p^* - p_r) = 2.303 \log(C_A t_{DA}) \quad (8)$$

or

$$p^* - p_r = 162.6 \frac{q_n \mu_w B_w}{kh} \log(C_A t_{DA}) = m \log(C_A t_{DA}) \quad (9)$$

where

$p_{D(MBH)}$ = dimensionless MBH pressure

p^* = extrapolated value of p_{ws} at infinite shut-in time (psia)

During the Long-Term Buildup Test, average reservoir pressure was approximated by the wellbore static pressure (p_{ws}) after sufficiently long shut-in.

Wellhead pressure recordings have been employed to estimate corresponding bottomhole values during the long-term shut-in period. When the well is shut-in:

$$p_{ws} = p_{ts} + \Delta p_{hydr} \quad (10)$$

where

p_{ts} = tubing-head shut-in pressure (psia)

Δp_{hydr} = hydraulic pressure difference (psia)

The value of Δp_{hydr} was estimated from actual measurements. Figure 8 shows that stabilized value of Δp_{hydr} is 6,515 psi during the Long-Term Buildup Test. The reason this value changes with time is most likely stablization of wellbore temperatures and densities. Table 2 shows the reservoir pressure calculated from Eqs. 7 and 9.

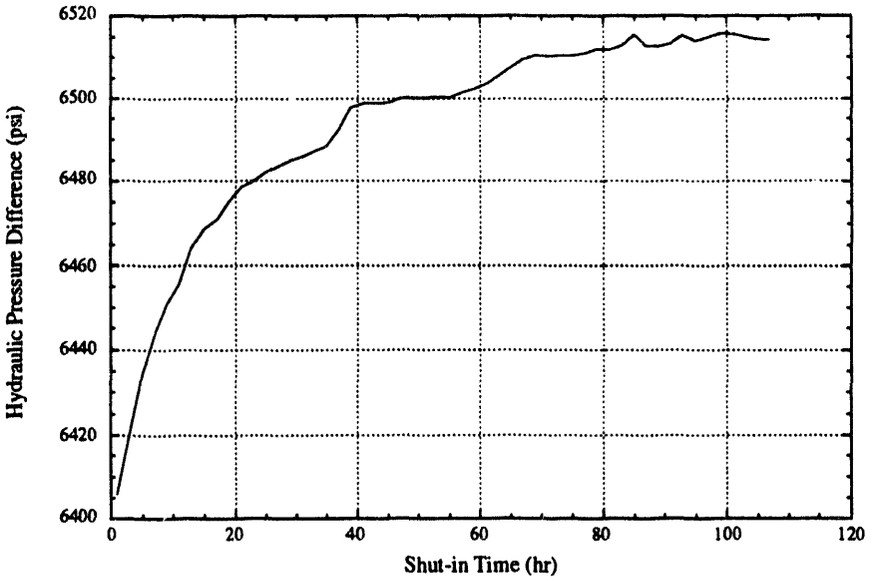

Fig. 8: Hydraulic pressure difference during Long-Term buildup test.

Table 2: Calculation of average reservoir pressure from buildup tests.

	RLT Buildup	79-hr Buildup	92-hr Buildup	LTT Buildup	'91 Buildup
m (psi/cycle)	15.5	29.5	19	15	9.5
kh (md-ft)	45,318	25,957	27,332	32,901	31,196
t_p (hr)	505	12,107	31,979	64,636	109,279
t_{DA}	2.072	28.449	79.126	192.516	306.61
p^* (psia)	12,599	11,345	10,549	10,301	12,110
p_r (psia)	12,613	11,338	10,536	10,285	12,098

Numerical Model of Gladys McCall Reservoir

In this section, work has focused on developing a hypothetical reservoir model that approximates the configuration of Gladys McCall reservoir geometry. Based on the drainage-shape estimation obtained in the previous section, various rectangular numerical models have been used to simulate the well transient pressure and pressure derivative behavior during the reservoir production period. A few distinguishable reservoir features observed in 1983 Reservoir Limits Test are recognized by a long, narrow reservoir model with the well located closer to one lateral side and to one end of the reservoir. A double-slope pressure behavior (on semilog pressure-time plot shown in Fig. 9) develops after the early radial flow period, which may indicate the presence of a no-flow boundary near the well. Following this period, linear flow character (square-root-time straight line shown in Fig. 10) becomes clear when two closer boundaries (possible parallel boundaries) are both felt at the well.

The short time pressure transient behavior of a well in a long, narrow reservoir is the same as that of an infinite reservoir, because at short time the well does not feel the effect of the boundaries. As shown previously in Fig. 5, a semilog plot of wellbore pressure vs. time yields a straight line from 0.2 hr to 0.65 hr, indicating early radial flow. As soon as effect of the nearest fault boundary is felt at the well, the well pressure deviates from this straight-line trend. A second straight line is observed in Fig. 9 (a magnified plot of Fig. 5). The slope of this line is almost precisely twice that of the early-time straight line. This is characteristic of pressure behavior shown by well in the vicinity of a sealing fault. The second flat portion of the pressure derivative plot shown in Fig. 6 confirms the doubling of slope. The distance to the fault, d, is obtained from the intersection-time, t_x, between these two straight lines by (Gray, 1965):

$$d = 0.01217 \sqrt{\frac{k\, t_x}{\phi \mu_w C_t}} \qquad (11)$$

which gives a distance of 280 ft for $t_x = 0.7$ hr shown on Fig. 9.

Linear flow solutions have been discussed extensively by many authors (Miller, 1962; Nabor, 1964; Kohlhaas and Abbott, 1982; Nutakki and Mattar, 1982; Ehlig-Economides and Economides, 1985; and Wong Ital., 1986). The transient linear flow for a constant rate case can be analyzed using the following equation:

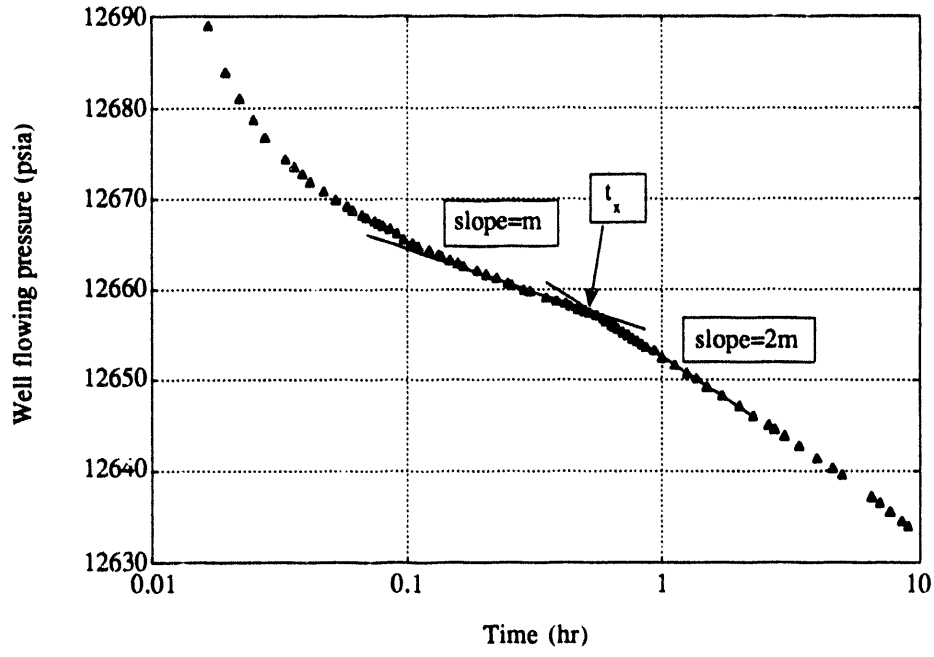

Fig. 9: 1993 Reservoir Limits Test wellbore pressure vs. flowing time.

$$p_i - p_{wf} = 8.129 \frac{q_p B_w}{h w} \sqrt{\frac{\mu_w}{\phi k C_t}} \sqrt{t} \qquad (12)$$

where p_i is initial reservoir pressure, p_{wf} is wellbore pressure, q_p is flow rate, w is reservoir width, h is the reservoir thickness, and C_t is the total system compressibility. According to this equation, a plot of wellbore flowing pressure vs. square root of flowing time yields a straight line of slope $8.129 \frac{q_p B_w}{h w} \sqrt{\frac{\mu_w}{\phi k C_t}}$, which allows a calculation of the channel width, w. The linear flow regime is also characterized by a half slope pressure derivative on the log-log plot. Figures 6 and 10 illustrate the linear flow characters, i.e., half slope log-log and square-root-time straight line, for RLT drawdown test on pressure derivative and wellbore pressure plots, respectively. The linear period occurs from approximately 8 hr to 18 hr with a square-root-time straight line slope of 7.01 psi/hr$^{1/2}$. A reservoir width of 1,900 ft is accordingly calculated. Nutakki (1982)

provides an equation to check the channel width calculation from the beginning time of the linear flow period, t_{LN}, as

$$t_{LN} = 1441\frac{\phi\mu_w C_t}{k} w^2 \qquad (13)$$

A t_{LN} value of 8 hr gives a channel width of 1,895 ft which confirms the previous calculation.

Based on above analysis, linear models with various sizes have been used to simulate the transient pressure and pressure derivative behavior of the 1983 RLT test. The model that matched best is 15,200 ft by 1,900 ft by 332 ft in dimension with the well located 4,500 ft to one end and 280 ft from one lateral side of the reservoir. Figure 11 shows a schematic diagram of the model. The drawdown and buildup pressure plots generated with the model are given in Figs. 12 and 13. They show good agreement with field data except those at small Δt . The discrepancies are caused by wellbore storage effects, which are not included in the model calculations. It is interesting to note that this numerical model resembles the reservoir model Rodgers ital. (1985) derived for the L. R. Sweezy geopressured reservoir in both size and shape. In their case, the model boundaries, identified from transient tests, are found located close to the geologic faults mapped in that region.

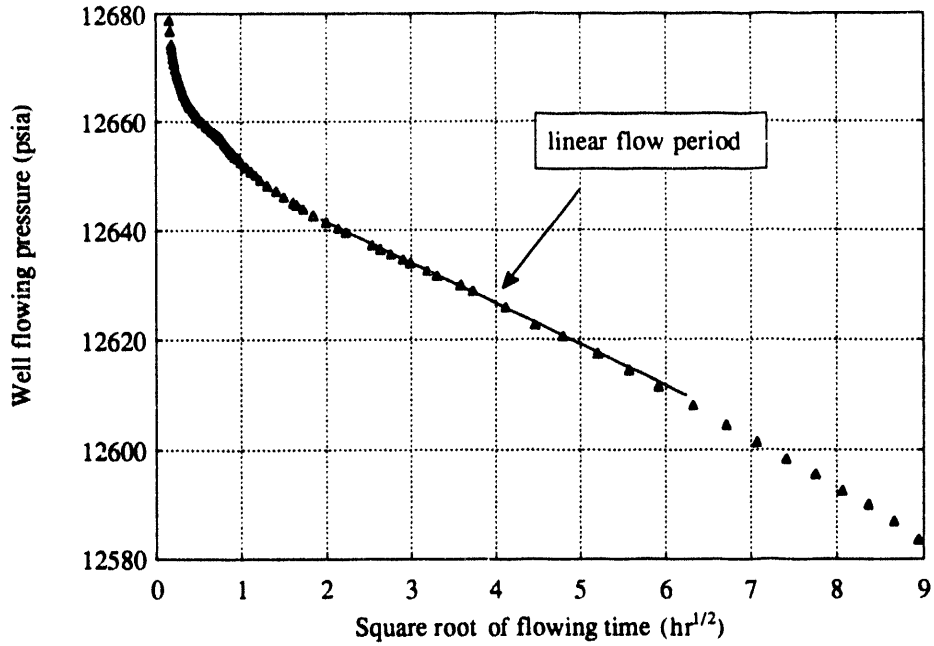

Fig. 10: 1983 Reservoir Limits Test wellbore pressure vs. square-root of flowing time plot.

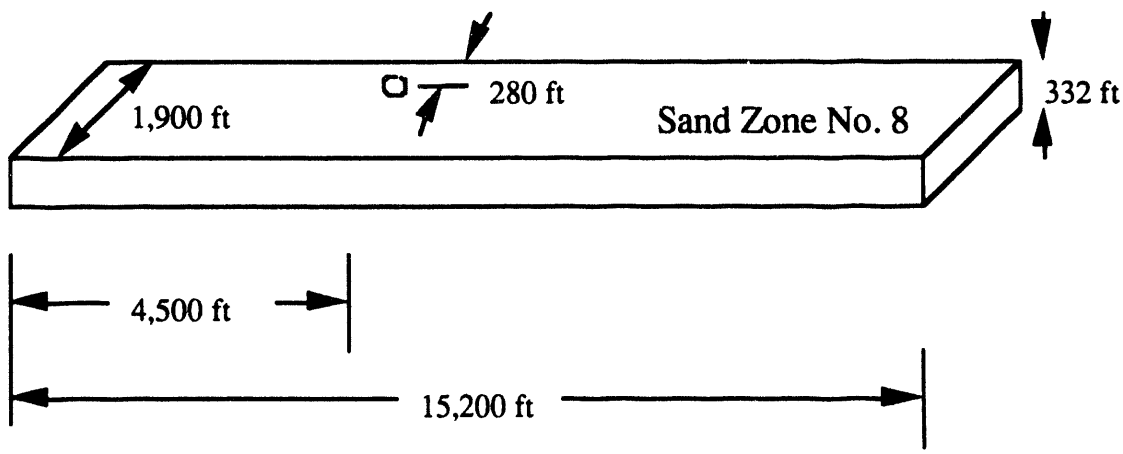

Fig. 11: Numerical model of Gladys McCall reservoir (15,200'× 1,900'× 332').

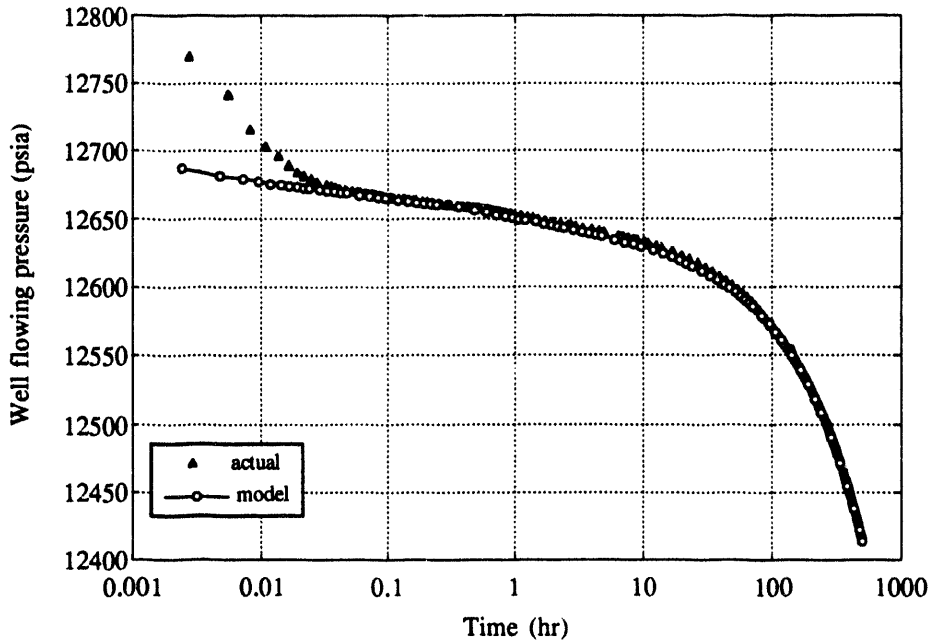

Fig. 12: RLT and model drawdown wellbore pressure vs. flowing time plot.

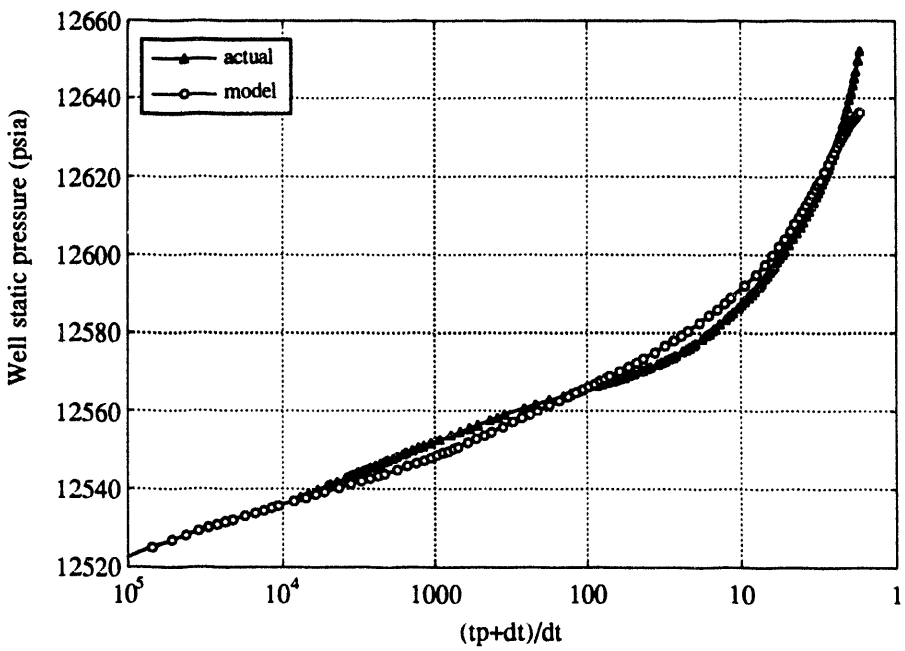

Fig. 13: RLT and model buildup pressure vs. Horner time plot.

RESERVOIR DRIVE MECHANISM

One important objective of this study was to determine which mechanism(s) might be responsible for observed pressure maintenance of the reservoir. With the fairly limited reservoir size indicated from the Reservoir Limit Test and the pressure recovery measured during the Long-Term Buildup, it is clear that some mechanism exists to supply water.

Models that match the downhole pressure measurement and the observed reservoir depletion behavior might be devised from any of the following reservoir drive mechanisms:

1. Stress-dependent rock formation compressibility
2. Long-term formation creep
3. Cross-flow from overlying/underlying sands
4. Shale water recharge
5. Leakage across boundaries
6. Free gas evolution

Earlier studies (Riney, 1988 and 1990) have eliminated 1, 4, and 6 as major mechanisms for Gladys McCall pressure maintenance based on parametric calculations and geological information. Riney assumed that cross-flow from sands overlying/underlying Sand Zone No. 8 was the major cause of pressure maintenance. However, because there was no geological reason to support recharge from such a spatial location, we treated this system more generally, as an aquifer-supported reservoir volume. Because none of the more conventional aquifer models could match the entire influx history of Gladys McCall reservoir, a conceptualized fault-controlled influx model has been developed based on material-balance calculations. It was assumed that water leaked through partially sealing fault(s) into the reservoir under steady-state conditions, and the conductivity of the fault depended on the pressure difference between the aquifer and the reservoir. This model showed a good match with reservoir influx data.

The actual water influx of Gladys McCall reservoir is calculated based on reservoir pressure and production data. The pressure behavior of a reservoir under water

drive is dependent upon the rate of reservoir fluid withdrawal and the rate of water encroachment. In response to a pressure drop in the reservoir, the surrounding aquifer supplies a source of water influx into the reservoir. A reservoir material balance equation can be written as

$$V_P C_t \frac{dp_r}{dt} = q_e - q_p B_w \tag{14}$$

where V_P is the reservoir pore volume, C_t is the total reservoir compressibility, p_r is the reservoir pressure, q_e is the rate of water influx, B_w is the brine formation volume factor, and $q_p$is the reservoir production rate. Integrating Eq. 14 with respect to time yields the cumulative reservoir water influx, We:

$$We(t) = \int_o^t q_e \, dt = - V_p C_t (p_i - p_r) + \int_o^t q_p \, dt \tag{15}$$

where p_i is the initial reservoir pressure. Equation 15 can be applied to quantify aquifer influx of Gladys McCall reservoir using the reservoir pressure and brine production tabulated in Tables 1 and 2. Figure 14 illustrates the results as a function of time. During the long-term reservoir production period (from October 7, 1983 to October 29, 1987), the well produced a total of 2.7×10^7 bbl brine, about one tenth of the reservoir pore volume. The reservoir pressure dropped from initially 12,784 psia (at datum 15,100 ft) to 10,285 psia. The corresponding water influx was 2.25×10^7 bbls. After the well was shut-in at 1,483 day (October 29, 1987), well pressure continually rose to values close to initial reservoir pressure due to strong and continuous water influx. The total amount of water provided from external sources is calculated to be 2.6×10^7 bbls prior to the 1991 drawdown test (Oct. 10, 1991).

In our study, three influx models commonly applied in evaluating the performance of hydrocarbon reservoirs have been investigated. The purpose is to identify the possible aquifer function of the Gladys McCall reservoir by matching the influx obtained from material-balance calculations. The flow of aquifer water into a reservoir is modeled in the same way as flow of oil from a reservoir into a well. Aquifer influx is calculated by solving the diffusivity equation using the pressure at the reservoir-aquifer contact as the aquifer inner boundary condition. It is assumed that the pressure at the reservoir-aquifer contact can be represented by the average reservoir pressure at all times.

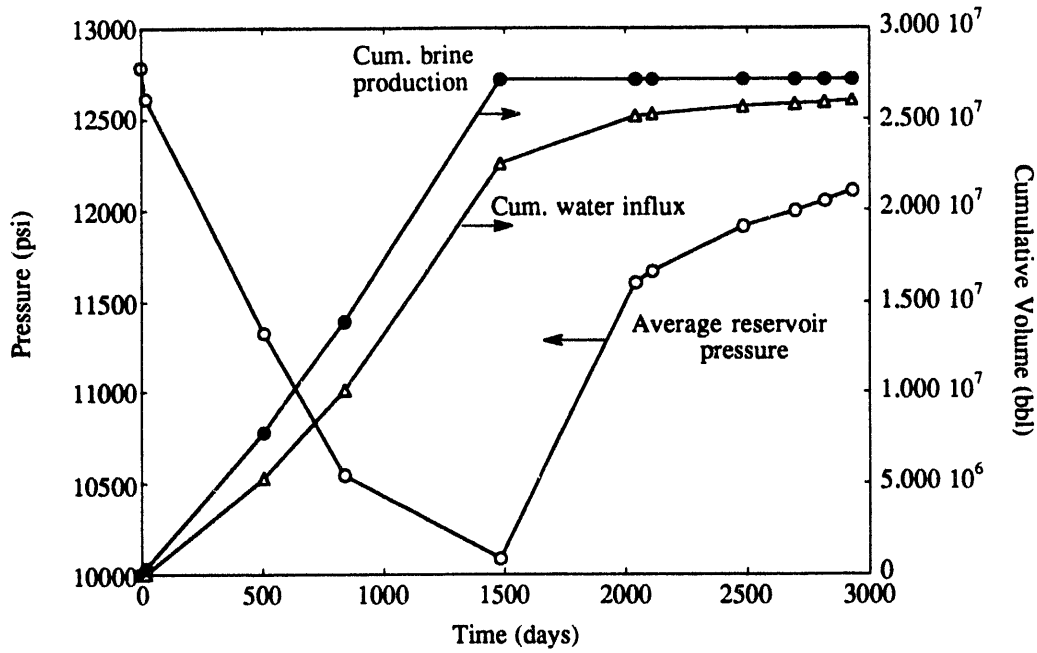

Fig. 14: Gladys McCall reservoir depletion and recovery history.

The conventional water influx models are:

1. Transient influx considering both radial (van Everdingen and Hurst, 1949) and linear (Miller, 1962; and Nabor, 1964) aquifer geometries.

2. Pseudosteady-state influx (Fetkovitch, 1971).

3. Steady-state influx (Schilthuis, 1936).

Cumulative water influx obtained from each method was compared with cumulative field influx to identify the possible influx model that could match Gladys McCall behavior.

Transient influx

van Everdingen and Hurst (1949) derived the constant terminal pressure solution for single-phase radial flow. The solution can be expressed in terms of cumulative water influx as:

$$W_e = U \Delta p W_D(t_D) \tag{16}$$

where U is the dimensional constant for aquifer geometry, Δp is the pressure drop at reservoir-aquifer boundary, W_D is the dimensionless cumulative water influx function for radial shaped aquifer, and t_D is the dimensionless time. Dake (1978) replotted van Everdingen and Hurst's W_D function as a function of dimensionless time for finite-bounded aquifer and infinite aquifer cases. The definitions of the dimensional geometry constant, U, and dimensionless time, t_D, were also given.

The water influx for a linear model can also be calculated using Eq. 16 by replacing the radial W_D function with a linear W_D function. Miller (1962) developed linear influx solutions for infinite and finite-sealed aquifers. Later, Nabor and Barham (1964) added the influx solution for a finite linear aquifer with constant pressure at the aquifer outer boundary.

To perform influx calculations, it is conventional to divide the reservoir pressure curve into a series of discrete time steps. Superimposing the step influxes gives the cumulative water influx. Vogt and Wang (1990) presented an accurate working formula for convolving Eq. 16 as:

$$We(t_{Dn}) = U \left[-W_D(t_{Dn}) \frac{p_1 - p_0}{t_{D1}} + \sum_{j=1}^{n-1} \left(\frac{p_j - p_{j-1}}{t_{Dj} - t_{Dj-1}} - \frac{p_{j+1} - p_j}{t_{Dj+1} - t_{Dj}} \right) W_D(t_{Dn} - t_{Dj}) \right] \tag{17}$$

where subscript j denotes the time step and n is the total number of time steps. Since all the variables required to calculate the water influx (Eq. 17) are unknown except the pressure, different sets of aquifer parameters have been tested through a trial and error procedure in order to match or to get close to the observed pressure behavior. In Figs. 15 to 19, transient influxes for radial and linear aquifers are plotted and compared to actual influx. A range of aquifer sizes (different values of U) and aquifer permeabilities

(different values of t_D) have been tested. The match is poor for both infinite models, especially for influx during the reservoir buildup period. Model results show that with the observed pressures, water migrates from the reservoir back to aquifer during this period resulting in decreasing cumulative water influx. This cannot physically occur. This is due to the fact that the aquifer transient flow takes a longer time to respond to the well shut-in at later times because of lengthening travel distance of the pressure response. This slows down aquifer influx. However, reservoir pressure still shows relatively rapid buildup in this period.

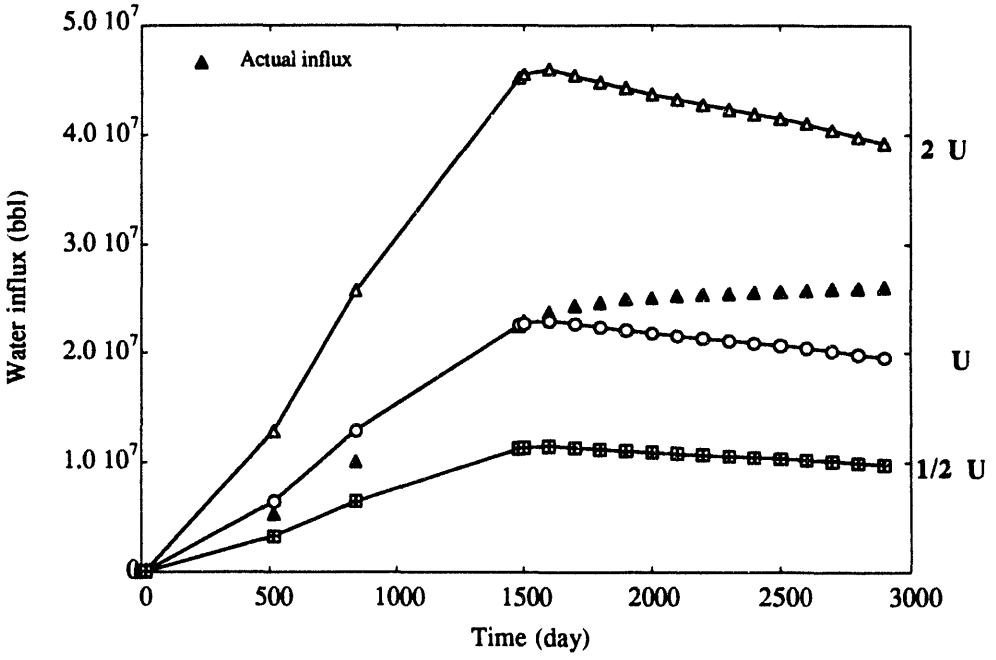

Fig. 15: Water influx for transient radial aquifer models with various aquifer sizes (U).

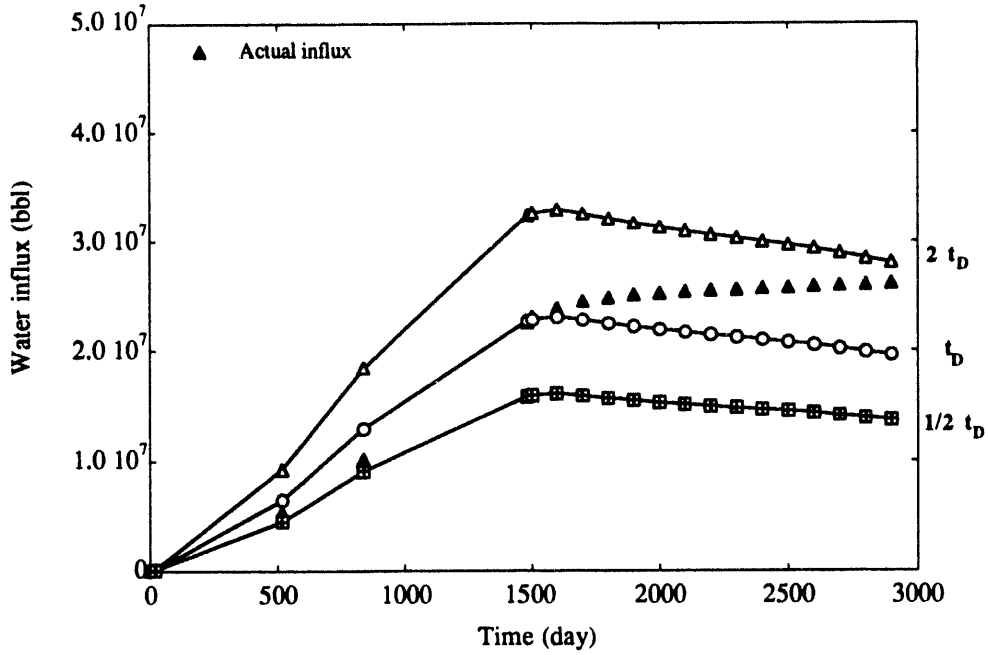

Fig. 16: Water influx for transient radial aquifer models with various aquifer permeabilities (t_D).

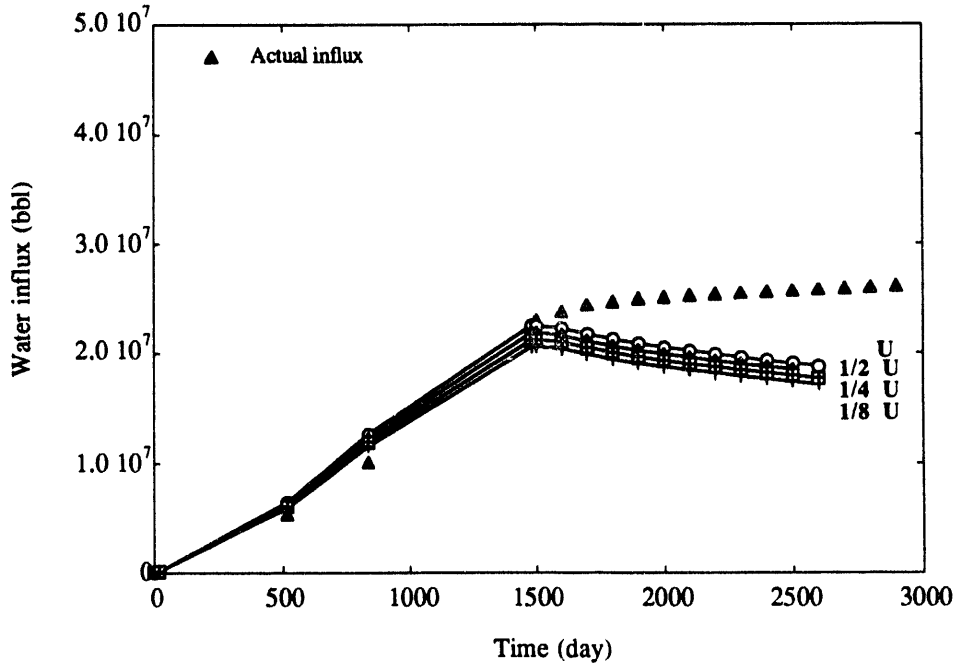

Fig. 17: Water influx for transient linear aquifer models with different aquifer sizes U (giving various aquifer lengths).

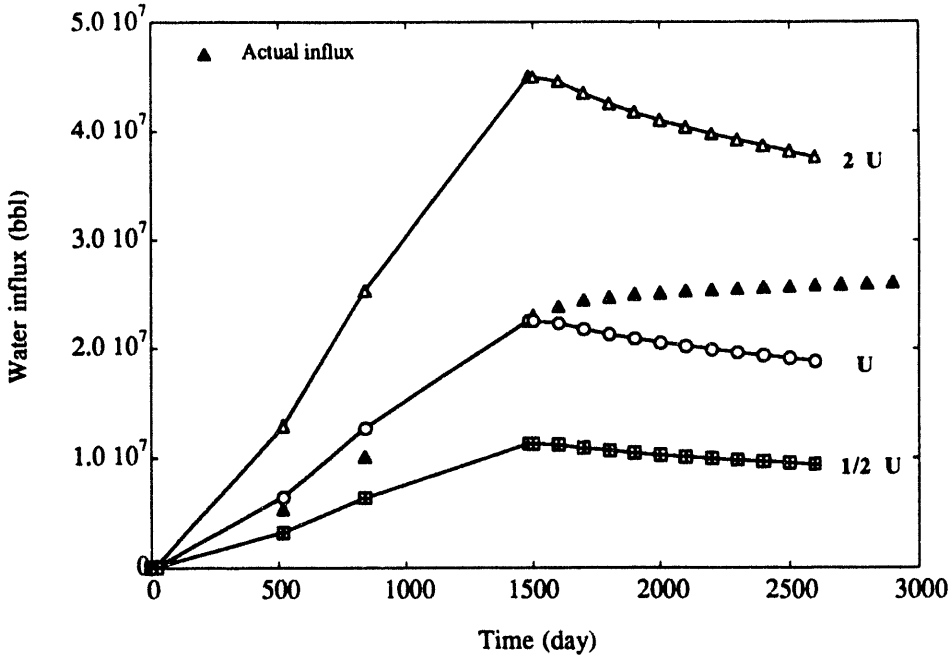

Fig. 18: Water influx for transient linear aquifer models with different aquifer sizes U (giving various cross-sectional areas of aquifer).

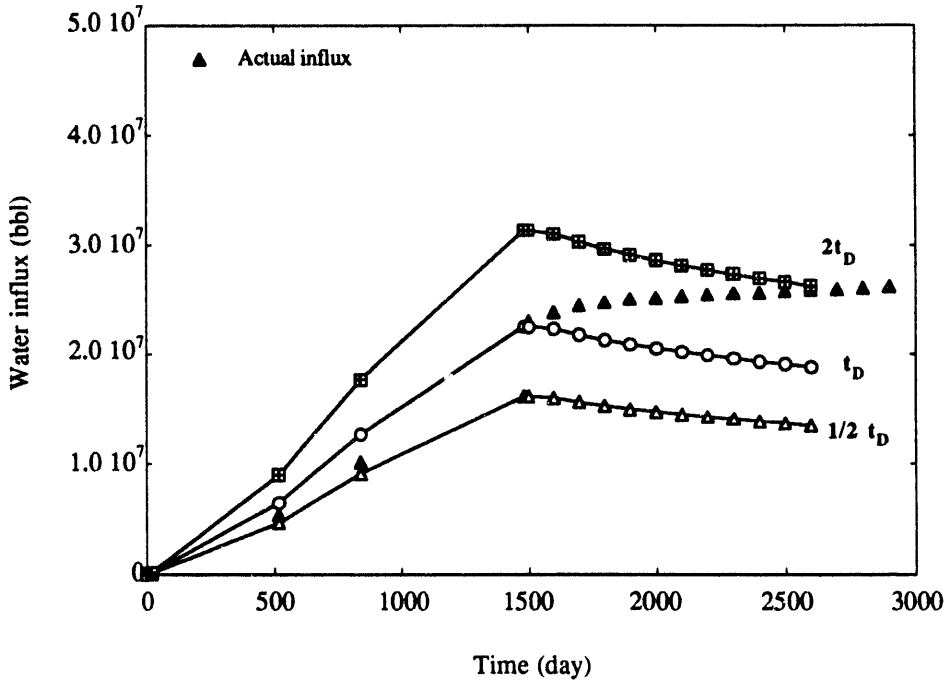

Fig. 19: Water influx for transient linear aquifer models with various aquifer permeabilities (t_D).

Pseudosteady-state influx

For an arbitrary geometry aquifer of finite extent in contact with a reservoir, it can be shown that at sufficiently large time the water influx rate reaches a pseudosteady-state (Fetkovitch, 1971) such that:

$$q_e = \frac{dWe}{dt} = J(p_a - p_r) \tag{18}$$

where J is the aquifer productivity index, p_a is the average aquifer pressure, and p_r is the average reservoir pressure. The working formula for pseudosteady-state influx can be found in Dake (1978). Figures 20 to 22 show results for various aquifer sizes and aquifer productivities. A relatively large aquifer can easily match the influx during the reservoir production period by choosing a proper value of J, but will overestimate the flux during the reservoir buildup period, as illustrated in Fig. 20 (J =7.3 curve). On the other hand, a small aquifer can improve the match of early buildup time, but eventually will undervalue the influx at later buildup time, as shown in Fig. 21 (15 times reservoir size curve). Figure 22 shows the influxes for aquifer sizes ranging from 15 to 20 times the reservoir size. None of these aquifer models can sustain sufficient influx at late buildup times.

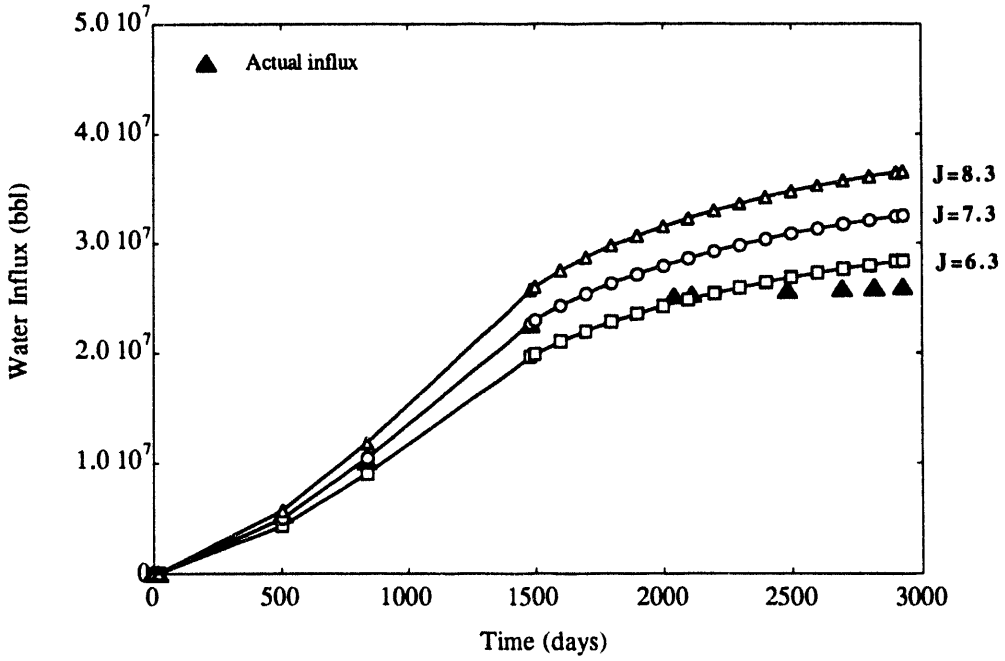

Fig. 20: Water influx for pseudosteady-state Fetkovitch models with various aquifer productivities, J. Aquifer size is 90 times reservoir size.

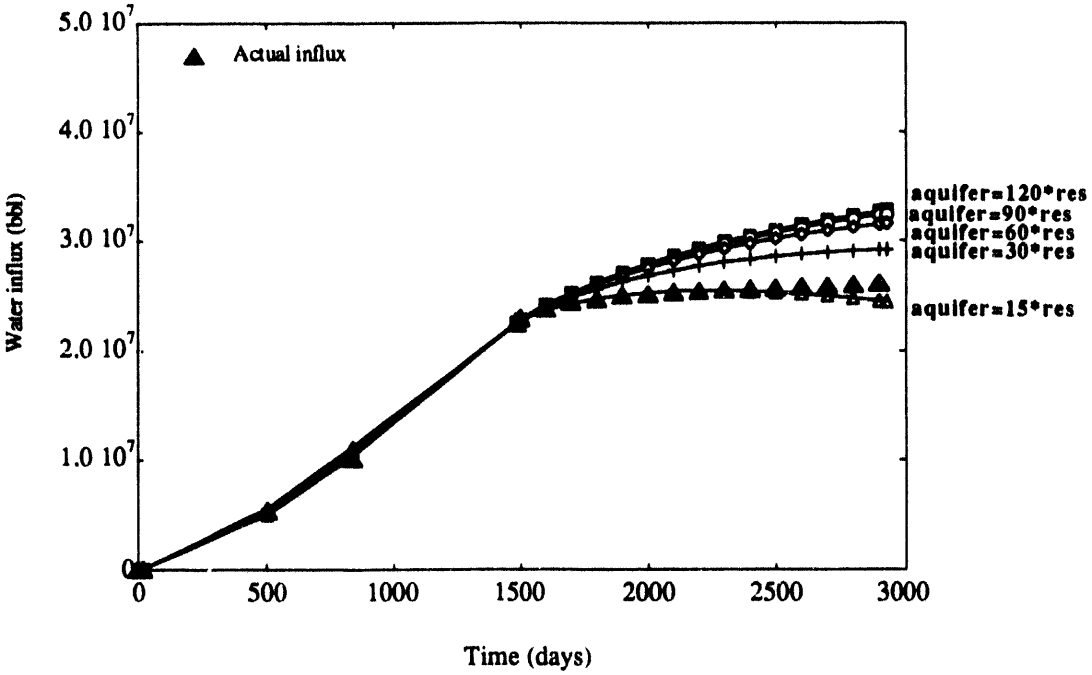

Fig. 21: Water influx for pseudosteady-state Fetkovitch models with various aquifer sizes and productivities, J.

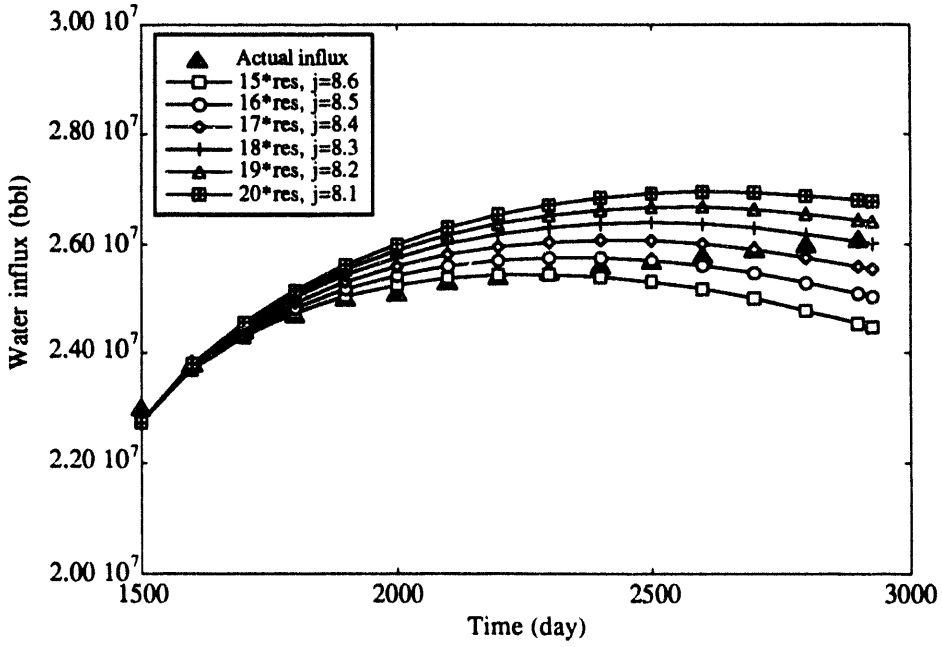

Fig. 22: Water influx for pseudosteady-state Fetkovitch models with various aquifer sizes and productivities, J.

Steady-state influx

For the steady-state influx model, the influx equation is similar to that of pseudosteady-state:

$$q_e = \frac{d\,We}{dt} = J\,(p_i - p_r) \tag{19}$$

where p_i is the initial aquifer/reservoir pressure. For a steady-state influx system, the aquifer pressure will remain at its initial pressure for all times. Again, a steady-state influx model with a J value of 7.3 bbl/day/psi matches the influx during the reservoir production period, but tends to overestimate the influx during the long-term buildup period (close to J =7.3 curve shown in Fig. 20).

It seems that the Gladys McCall aquifer acted differently during the production and buildup periods. There is no single conventional influx model which can fit the entire field influx history. Realizing that the aquifer influx may be controlled by a partially sealing fault at the aquifer-reservoir boundary, a hypothetical steady-state influx model has been developed in which the degree of fault open to flow depends on the pressure difference between the aquifer and the reservoir.

Faults are zones of weakness in the formation. While under abnormal pressure (geopressured) conditions, the uneven pressure across the fault due to fluid withdrawal may easily trigger the movement of the fault to open a conductive pathway by stress-releasing. The pressure-dependent fluid-conductive fault model was successfully used by Shook (1992) to match the production history of the Pleasant Bayou reservoir. Here, a good match is also achieved with the fault-controlled influx model developed for Gladys McCall reservoir, as shown in Fig. 23. Figure 24 illustrates the J-function vs. time used for the match. In our influx model, the non-sealing fault(s) acts like a flow-controlling valve. The amount of water influx is dependent on both the fault conductivity and the pressure difference between the aquifer and the reservoir. The opening-up and closing-down of the fault, which determine the fault conductivity, are also dependent on the pressure difference across the fault, Δp_{fault}.

To evaluate the fault-controlled steady-state influx, Eq. 19 is still applied, but the aquifer productivity index, J, varies with $(p_a - p_r)$. The J values which match the entire Gladys McCall influx history reveal certain pressure-dependent features that may indicate fault activation caused by fluid withdrawal on one side of the fault. As shown in Fig.

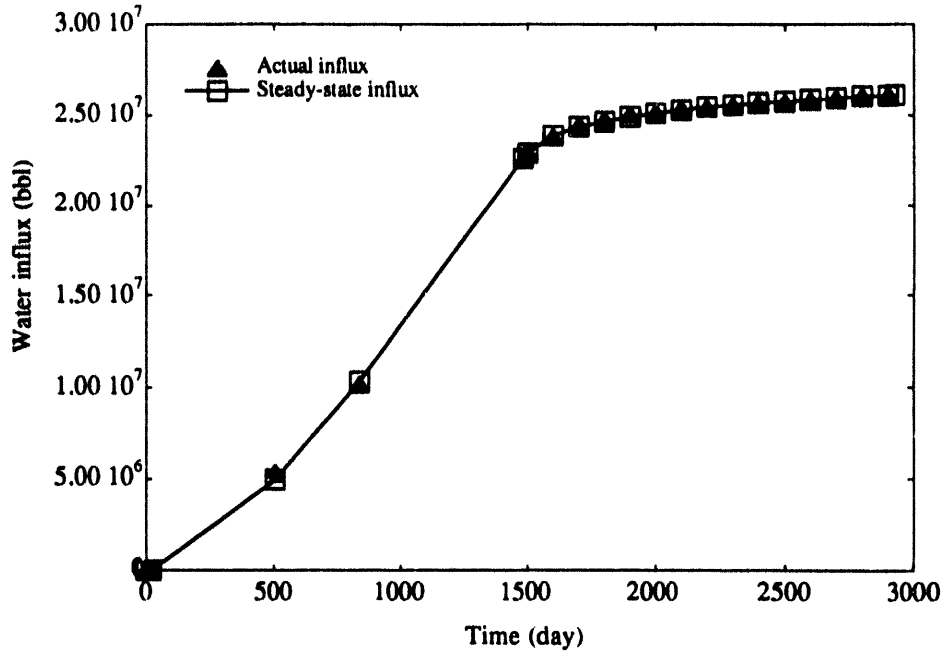

Fig. 23: Steady-state fault-controlled influx model results and Gladys McCall influx.

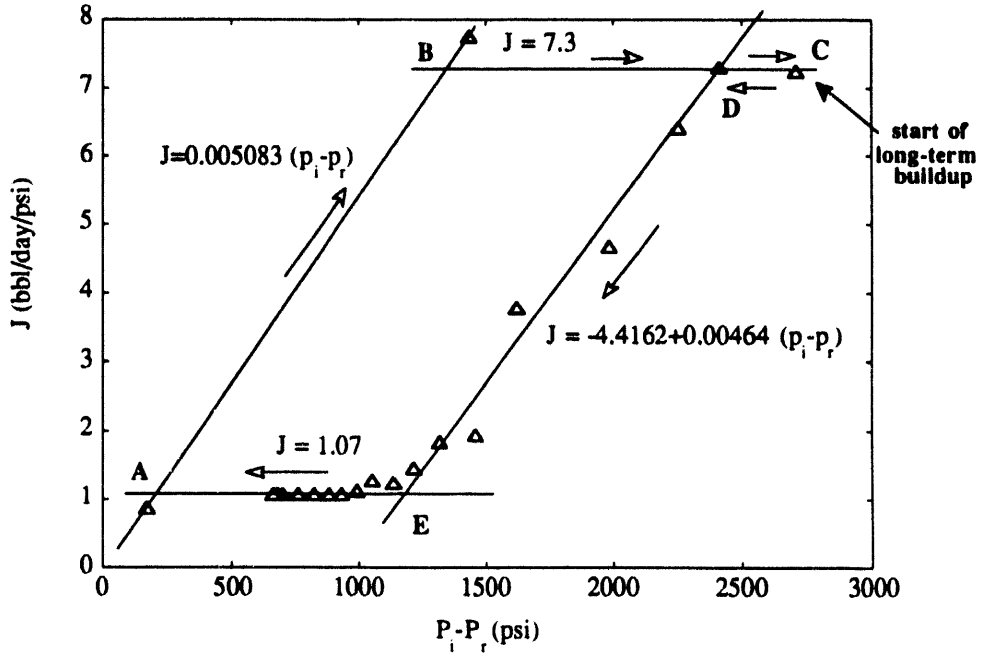

Fig. 24: Fault transmissibility plotted as functions of pressure difference between reservoir and aquifer (steady-state influx).

24, shortly after the Gladys McCall Reservoir started production, the fault opened. Following A-B, the fault conductivity increased continually to a maximum value of 7.3 bbl/day/psi with the increase of the pressure difference, Δp_{fault}, to 1,300 psia. Once fault opened to its maximum extent (point B), its conductivity remained at a constant value regardless of further increases of the pressure difference (along B-C). At the time well was shut in (point C), water influx held on the maximum possible rate for a short while. When Δp_{fault} fell below 2,350 psia, the fault began to close (point D). J started decreasing and decreased linearly with the decline of Δp_{fault} (D-E). However, the fault didn't close fully. During the late time of the long-term buildup period, the fault system maintained steady-state water leakage into the reservoir with a minimum constant fault conductivity of 1.07 bbl/day/psia, which closes to the J value obtained at the beginning of reservoir production period (J =0.97 bbl/day/psia).

Figure 24 suggests a hysteresis loop for fault conductivity during the reservoir production and shut-in periods. The fault may also have finite conductivity initially. This is difficult to determine because of limited data at early times. And, since the data points available for constructing the J functions were limited, some of the straight-line relations between the fault conductivity and the pressure difference had to be drawn from direct interpolation. To validate the J functions shown in Fig. 24, we made a simple material-balance calculation by placing the J functions back into Eq. 15 for a reverse evaluation of $(p_i\text{-}p_r)$ or Δp_{fault}. The reservoir production period was approximately divided into two constant-rate production periods (q_p =14,160 bbl/day and q_p =20,800 bbl/day). Figure 25 illustrates the comparison of the results with reservoir data. The match is reasonably good.

Our next step is to use the J functions to predict aquifer influx and reservoir pressure performances for various reservoir production rates. Shown in Fig. 26 are the pressure differences, Δp_{fault}, plotted as a function of time for four constant production rate cases. All of these curves illustrate that reservoir pressure drops rapidly at initial time because of high volume of brine production and lack of influx. However, the influx rate increases as the pressure difference increases, and eventually matches the brine production rate (as indicated by the plateau on each curve). With this model the withdrawal rate cannot be larger than around 25,000 bbl/day. Otherwise it will cause the reservoir pressure (p_i =12,784 psia) drops below bubble point pressure. Dissolved

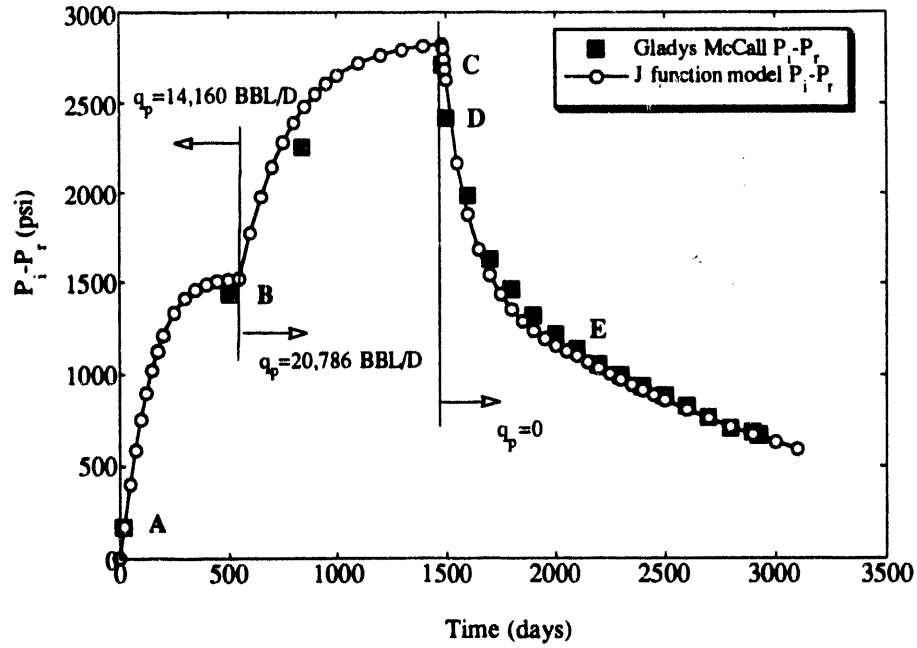

Fig. 25: Pressure difference between the reservoir and the aquifer as a function of time. Both reservoir data and *J*-function model data are included.

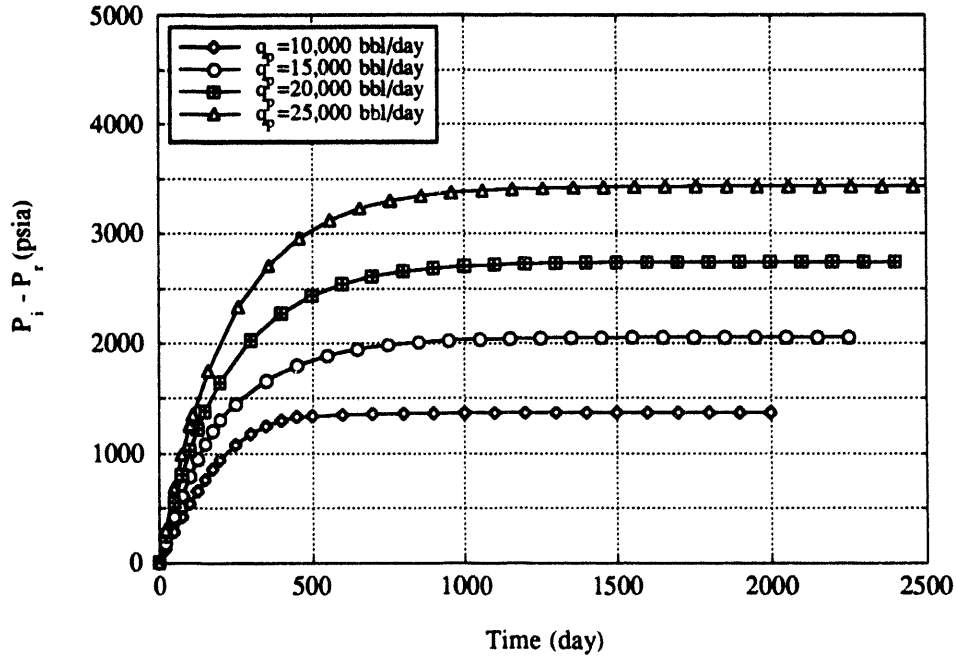

Fig. 26: Pressure behavior as a function of brine production rate, steady-state influx.

hydrocarbon gas then evolves from the liquid phase and becomes movable in the reservoir. The single-phase influx model will be no longer valid under these conditions.

The fault-controlled steady-state influx model provides a possible explanation of the unconventional aquifer behavior of the Gladys McCall reservoir. However, it does not quantify either the capacity and productivity of the aquifer, or the factors that influence the flow-induced fault movement. Additional data from geological mapping, seismic analysis, rock-stress studies, and fault-activation monitoring are needed for a better description of the Gladys McCall reservoir/aquifer system, as well as a better understanding of the aquifer-influx mechanisms in the geopressured region. In another geopressured reservoir model (Rodgers Ital., 1985), the rapid pressure response of the aquifer to the fluid production is attributed to large formation compressibility. Under abnormal pressure conditions, the formation porosity shrinks quickly as fluid is withdrawn from the pore spaces, resulting in less pressure decline. Therefore, in their study, rock compaction is considered the primary energy drive mechanism of the tested aquifer. The effect of rock compressibility is not considered in our transient pressure analysis or influx calculations.

CONCLUSIONS

Transient pressure analysis techniques have been used to evaluate the performance of the Gladys McCall Geopressured-Geothermal reservoir. An aquifer influx model has also been developed based on reservoir material-balance calculations.

The transient pressure analysis indicates that the connected pore volume of the reservoir is about 2.70×10^8 bbls. This analysis also indicated that the reservoir shape is probably long and thin with the well considerably off-center. An elongated numerical reservoir model developed accordingly was able to reproduce the pressure characteristics shown in the Reservoir Limits Test. Additional geological investigations need to be made to confirm the reservoir configurations.

Earlier studies assumed that crossflow from sands overlying/underlying Sand Zone No. 8 was the major cause of reservoir pressure maintenance. In this study, leakage across unknown reservoir boundaries is believed to be an important mechanism.

A fault-controlled steady-state influx model has been developed to account for the pressure support during both reservoir depletion and recovery phases. The influx rate and the fault conductivity were found to be functions of the pressure difference between the aquifer and the reservoir. In addition, the stress-induced hysteresis in formation rock were highlighted by the differences between reservoir unloading (depletion) and loading (recovery) fault conductivities.

The fault-controlled fault influx analysis is based purely on a fluid flow model which does not include the effects of rock properties. Formation stress analysis along fault zones and reservoir-scale rock mechanics studies may be needed for locating the leaky fault as well as for quantifying the fault movement due to stress difference. Investigation of the effect of rock compressibility on pressure maintenance may provide an explanation of aquifer driving energy for steady-state or near steady-state influx. Additional long-term drawdown tests may also help to determine the dimension and the deliverability of the pressure-supporting aquifer.

NOMENCLATURE

A = area, ft^2

B_w = water formation volume factor , bbl/stb

C_A = Dietz shape factor, dimensionless

C_t = total system compressibility, psi^{-1}

C_w = water compressibility, psi^{-1}

h = reservoir thickness, ft

J = aquifer productivity index, bbl/day/psi

k = permeability, md

kh = transmissivity, md-ft

m = slope of linear portion of semilog plot, psi/cycle

m^* = slope of straight line on a linear plot of p_{wf} vs. t , psi/hr

p^* = extrapolated value of p_{ws} at infinite close-in time, psia

p_{1hr} = pressure at Δt = 1 hr extrapolated from the straight line, psia

p_b = bubble point pressure, psia

$p_{D(MBH)}$ = dimensionless MBH pressure

Δp_{hydr} = hydraulic pressure drop, psia

p_i = initial pressure, psia

p_{int} = pressure at intercept, psia

p_r = average reservoir pressure, psia

p_{ts} = tubing-head shut-in pressure, psia

p_{wf} = bottomhole flowing pressure, psia

q_p = average flow rate, stb/day

Q = cumulative production, bbl

q_e = water influx rate, bbl/day

q_n = constant rate just before shut-in, bbl/day

q_w = water flow rate, bbl/day

r_w = wellbore radius, ft

S = skin factor, dimensionless

t_{DA} = dimensionless time

$(t_{DA})_{pss}$ = dimensionless time at the beginning of pseudosteady-state flow

t_p = equivalent flow time, hr

t_{pss} = time at the beginning of pseudosteady-state flow, hr

V_p = reservoir drainage volume, bbl

W_e = cumulative water influx, bbl

ϕ = porosity, dimensionless

μ_w = water viscosity, cp

ρ_w = water density, lbm/ft^3

APPENDIX A

Shown in Appendix A are the pressure derivative plots for Gladys McCall transient tests and three numerical models.

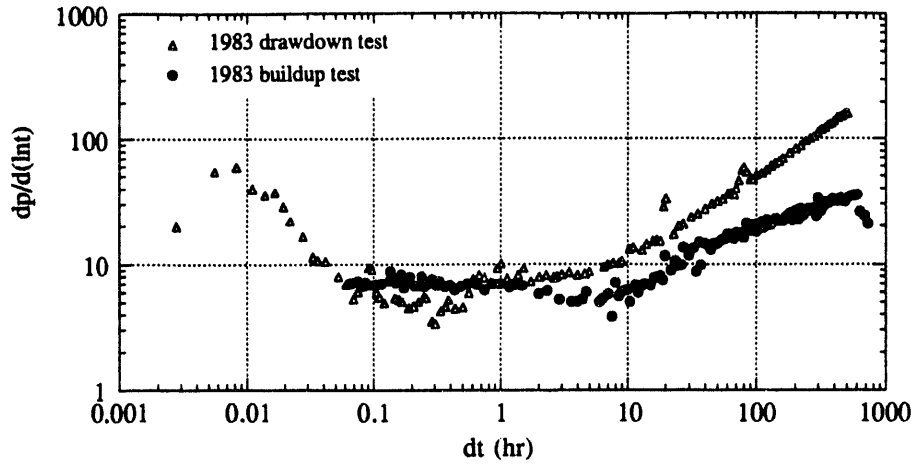

Fig. A-1: Pressure derivative plots of 1983 drawdown and buildup tests.

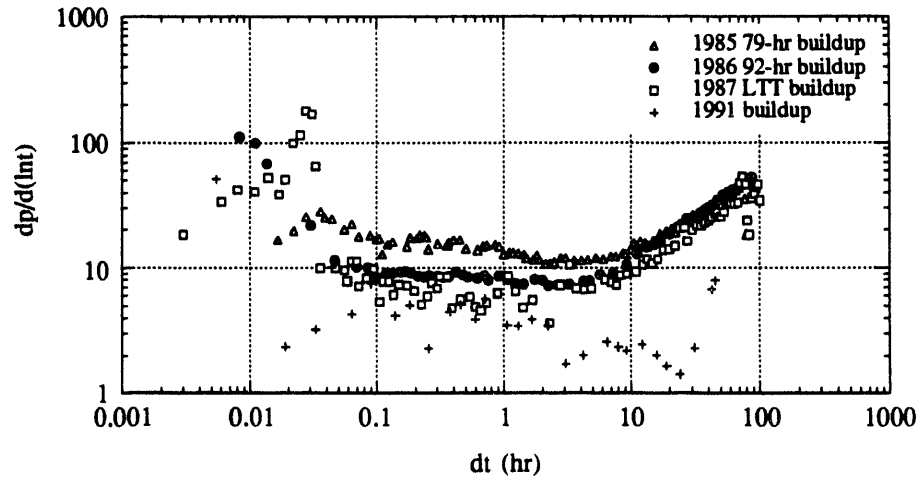

Fig. A-2: Pressure derivative plots of 1985—1991 buildup tests.

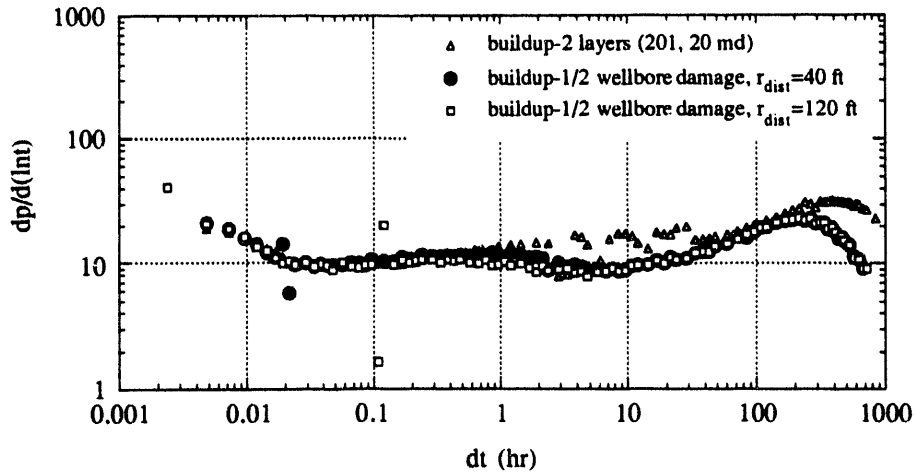

Fig. A-3: Results of three 15,200' × 1,900 ' × 332' numerical models:
i) two layers without cross flow (201 and 20 md)
ii) half of the wellbore damaged to 120' (into the formation)
iii) half of the wellbore damaged to 40' (into the formation).

REFERENCES

Ambastha, A.K., McLeroy, P.G., and Grader, A.S.: "Effects of A Partially Communicating Fault in A Composite Reservoir on Transient Pressure Testing," *SPE Form. Eval.* (June 1989) 210-18.

Bourdet, D.B., Whittle, T.M., Douglas, A.A., and Pirard, Y.M.: "A New Set of Type Curves Simplifies Well Test Analysis," *World Oil* (May 1983) 95.

Dake, L.P.: *Fundamentals of Reservoir Engineering,* Elsevier Scientific Co., Amsterdam (1978).

Earlougher, R.C., Jr.: *Advances in Well Test Analysis,* SPE of AIME, Dallas, TX (1977).

Earlougher, R.C., Jr. and Ramey, H.J., Jr.: "Interference Analysis in Bounded Systems," *J. Cdn. Pet. Tech.* (Oct.-Dec. 1973) 33-45.

Ehlig-Economides, C: "Use of the Pressure Derivative for Diagnosing Pressure-Transient Behavior," *J. Pet. Tech.* (Oct. 1988) 1280-82.

Ehlig-Economides, C. and Economides, M.J.: "Pressure Transient Analysis in an Elongated Linear Flow System," *Soc. Pet. Eng. J .* (Dec. 1985) 839-47.

Fetkovich, M.J.: "A Simplified Approach to Water Influx Calculations - Finite Aquifer Systems," *J. Pet. Tech.* (July 1971) 814-28.

Gray, K. E.: "Approximating Well-to-Fault Distance From Pressure Buildup Tests," *J. Pet. Tech.* (July 1965) 761-67.

Horne, R. N.: *Modern Well Test Analysis, A Computer-Aided Approach*, Petroway Inc, Palo Alto, CA (1990).

John, C. J.: "Geology of the Gladys McCall Geopressured Prospect, Cameron Parish, Louisiana," *J. Energy Resources Tech.* (Dec. 1988) 255-61.

Kohlhaas, C.A. and Abbott, W.A.: "Application of Linear and Spherical Flow Analysis Techniques to Field Problems-Case Studies," paper SPE 11088 presented at the 1982 Annual Fall Technical Conference and Exhibition of the Society of Petroleum Engineers of AIME, New Orieans, LA, Sept. 26-29.

Kutasov, I. M.: "Correlation Simplifies Obtaining Downhole Brine Density," *Oil & Gas J.* (Aug 5, 1991) 48-49.

McCain, W. D. Jr.: "Reservoir Fluid Property Correlations — State of Art," *SPE Res. Eng.* (May 1991) 266-72.

Meehan, D. N.: "Estimating Water Viscosity at Reservoir Conditions," *Petroleum Eng.* (Nov. 1980) 117-18.

Meehan, D. N.: "A Correlation for Water Compressibility," *Petroleum Eng.* (Nov., 1980) 125-26.

Miller, F.G. : " Theory of Unsteady-State Influx of Water in Linear Reservoirs," *J. Inst. Pet.*, **48**, 467 (Nov. 1962) 365-79.

Nabor, G.W.: "Linear Aquifer Behavior," *J. Pet. Tech.* (May 1964) 561-3.

Numbere, D., Brigham, W. E., and Standing, M. B.: *Correlation of Physical Properties of Petroleum Reservoir Brines*, Stanford University Petroleum Research Institute (1977).

Nutakki, R. and Mattar, L.: "Pressure Transient Analysis of Wells in Very Long Narrow Reservoirs," paper SPE 11221 presented at the 1982 Annual Fall Technical Conference and Exhibition of the Society of Petroleum Engineers of AIME, New Orieans, LA, Sept. 26-29.

Osif, T. L.: "The Effects of Salt, Gas, Temperature, and Pressure on the Compressibility of Water," paper SPE 13174 presented at the 1984 SPE Annual Technical Conference and Exhibition, Houston, Sept. 16-19.

Ostermann, R. D., Bloori, A., and Dehghani, K.: "The Effect of Dissolved Gas on Reservoir Brine Viscosity, paper SPE 14211 presented at the 1985 SPE Annual Technical Conference and Exhibition," Las Vegas, Sept. 22-25.

Price, L. C., Blount, C. W., Gowan, D. M., and Wenger, L.: "Methane Solubility in Brines with Application to the Geopressured Resource," *Proc. Fifth Conference on Geopressured-Geothermal Energy*, Louisiana State University, LA (1981) 205-14.

Riney, T.D.: "Gladys McCall Geopressured Reservoir Analysis," *J. Energy Resources Tech.* (Dec. 1988) 262-68.

Riney, T.D.: *Depletion and Recovery Behavior of the Gladys McCall Geopressured Geothermal Reservoir*, Topical Report NO. SSS-TR-9011474, U.S. Department of Energy (1990).

Rodgers, J.S., Coble, L.E., and Hamilton, J.R.: "Analysis of DOW/DOE No.1 L. R. Sweezy Well Tests," *Proc. Sixth Conference on Geopressured-Geothermal Energy*, The University of Texas at Austin, Texas (1985) 57-70.

Schilthuis, R.J.: "Active Oil and Reservoir Energy," *Trans.*, AIME (1936) **118**, 33-37.

Shook, G.M.: *An Integrated Approach to Reservoir Engineering at Pleasant Bayou Geopressured-Geothermal Reservoir*, Topical Report No. DE-AC07-761D01570, U.S. Department of Energy (Dec. 1992).

Wallace, R.H., Jr.: "Geopressured-Geothermal Resources in the Northern Gulf of Mexico Basin: An Overview," *Geopressured-Geothermal Energy Resource Appraisal,* Louisiana Geological Survey Guidebook Series No. 2, 49-71.

Westhusing, J.K. and Goldsberry, F.L.: "The Gladys McCall Design Well Project," *Geopressured-Geothermal Energy Resource Appraisal,* Louisiana Geological Survey Guidebook Series No. 2, 79-111.

Wong, D.W., Mothersele, C.D., and Harrington, A.G.: "Pressure Transient Analysis in Finite Linear Reservoirs Using Derivative and Conventional Techniques: Field Examples," paper SPE 15421 presented at the 1986 Annual Fall Technical Conference and Exhibition of the Society of Petroleum Engineers of AIME, New Orl eans, LA, Oct. 5-8.

van Everdingen, A.F., and Hurst, W.: "The Application of the Laplace Transformation to Flow Problems in Reservoirs," *Trans.*, AIME (1949) **186**, 305-24.

Vogt, J.P. and Wang, B.: "A More Accurate Water Influx Formula with Applications," *J. Can. Pet. Tech.* (July-Aug. 1990) **29**, 4, 52-62.